3-10-2008

Mesoporous Silica Nanoparticles Inhibit Cellular Respiration

Zhimin Tao
Upstate Medical University, State University of New York

Tewodros Asefa
Syracuse University

Cole Duncan
Syracuse University

Abhishek Anan
Syracuse University

Jerry Goodisman
Syracuse University

NANO LETTERS

2008
Vol. 8, No. 5
1517-1526

Mesoporous Silica Nanoparticles Inhibit Cellular Respiration

Zhimin Tao,[†] Matthew P. Morrow,[†] Tewodros Asefa,[‡] Krishna K. Sharma,[‡] Cole Duncan,[‡] Abhishek Anan,[‡] Harvey S. Penefsky,[§] Jerry Goodisman,[*,‡] and Abdul-Kader Souid[*,†]

Department of Pediatrics, State University of New York, Upstate Medical University, 750 East Adams Street, Syracuse, New York 13210, Department of Chemistry, Syracuse University, CST, 1-014, Syracuse, New York 13244, and Public Health Research Institute, 225 Warren Street, Newark, New Jersey 07103

Received January 25, 2008; Revised Manuscript Received March 10, 2008

ABSTRACT

We studied the effect of two types of mesoporous silica nanoparticles, MCM-41 and SBA-15, on mitochondrial O_2 consumption (respiration) in HL-60 (myeloid) cells, Jurkat (lymphoid) cells, and isolated mitochondria. SBA-15 inhibited cellular respiration at 25–500 μg/mL; the inhibition was concentration-dependent and time-dependent. The cellular ATP profile paralleled that of respiration. MCM-41 had no noticeable effect on respiration rate. In cells depleted of metabolic fuels, 50 μg/mL SBA-15 delayed the onset of glucose-supported respiration by 12 min and 200 μg/mL SBA-15 by 34 min; MCM-41 also delayed the onset of glucose-supported respiration. Neither SBA-15 nor MCM-41 affected cellular glutathione. Both nanoparticles inhibited respiration of isolated mitochondria and submitochondrial particles.

Nanoparticles have been suggested for cellular drug (or gene) delivery and other important biological applications.[1–3] Consequently, their potential adverse effects on human health have attracted much attention. The term "nanotoxicology" is now commonly used to describe cellular injuries produced by various nanoparticles.[2] For example, treatment of T-cells with multiwalled carbon nanotubes (20–40 nm diameter and 1–5 μm length) caused dose- and time-dependent apoptosis.[4] Water-soluble fullerene nanoparticles can transfer electrons to O_2, producing reactive O_2 species (ROS) and lipid membrane peroxidation.[5] Silica nanoparticles induce mitochondrial oxidative stress and deplete cellular glutathione (GSH).[6] Many of these cytotoxic effects can be visually confirmed by atomic force microscopy.[7]

Cytotoxins block cellular respiration (mitochondrial O_2 consumption) by a variety of mechanisms. In toxin-induced apoptosis,[8–10] the intracellular process is mediated by a series of cysteine, aspartate-directed proteases, termed caspases. Caspase activation leads to mitochondrial dysfunction, which includes opening of the permeability transition pores, collapse of the mitochondrial membrane potential, and uncoupling of oxidative phosphorylation.[11] Other potential deleterious actions include toxin-induced direct mitochondrial injury, inhibition of metabolism, and blocking mitochondrial fuel delivery.

Systematic investigation of the cytotoxicity of nanomaterials is essential prior to their medical application. Considering the special behavior at nanoscale, changes in particle material, size, shape, surface area, aggregation, and conjugation are expected to alter nanoparticles' biological effects. MCM-41 nanospheres have been shown to efficiently enter cells and induce significant toxicity.[12,13] This study investigates the effects of MCM-41 and SBA-15 mesoporous silica nanoparticles on cellular bioenergetics (cellular respiration and ATP content). These nanomaterials are currently considered as potential vehicles for drug and neurotransmitter deliveries.[14–16] We show that the mesoporous silica nanomaterials affect mitochondrial function, in a manner dependent on their physical properties.

MCM-41 and SBA-15 mesoporous silica nanoparticles were made by supramolecular self-assembly techniques under base- and acid-catalyzed conditions, respectively.[17–19] The transmission electron microscopy (TEM) images (Figure 1) show MCM-41 materials are rather regular spheres (300–650 nm in diameter), while SBA-15 materials are irregularly shaped with dimensions of hundreds of nanometers. The materials were characterized by powder X-ray diffraction (XRD), which showed sharp low-angle Bragg reflections and highly ordered mesostructures (see Supporting Information,

* To whom correspondence should be addressed: (J.G.) tel 315-443-3035, fax 315-443-4070, e-mail goodisma@mailbox.syr.edu; (A.-K.S.) tel 315-464-5294, fax 315-464-7238, e-mail souida@upstate.edu.

† Department of Pediatrics, State University of New York, Upstate Medical University.

‡ Department of Chemistry, Syracuse University.

§ Public Health Research Institute.

10.1021/nl080250u CCC: $40.75
Published on Web 04/01/2008

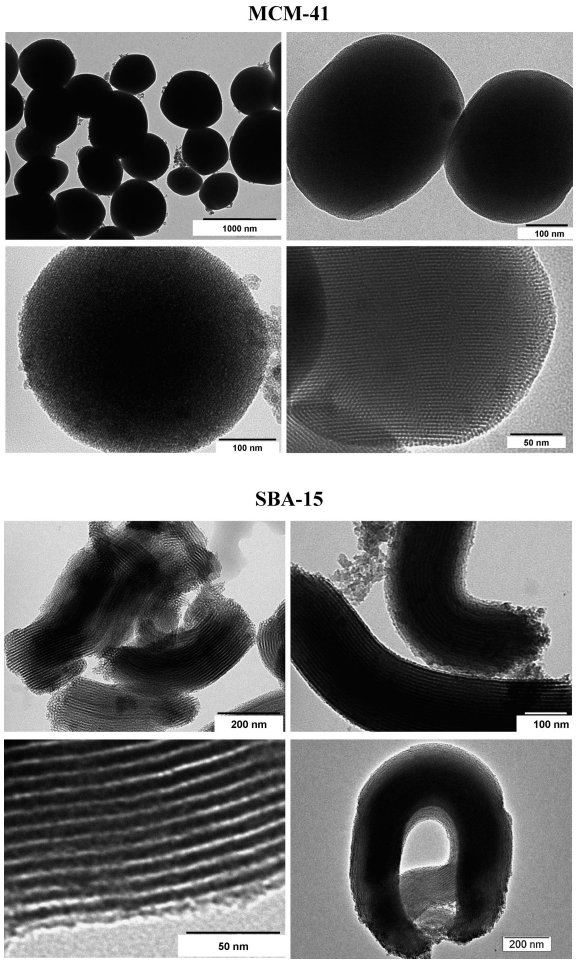

Figure 1. TEM images of MCM-41 and SBA-15.

Figure S1). The lattice spacing for MCM-41 was ~44 Å and that for SBA-15 was ~106 Å. The nitrogen gas adsorption isotherm (NGAI) profiles for both materials showed type IV isotherms with steep capillary condensation steps (see Supporting Information, Figures S2A and S3A), confirming highly ordered mesoporous particles with large surface areas. From the NGAI measurements, MCM-41 and SBA-15 have BET surface areas of 821 and 506 m^2/g, respectively, and monodisperse pore size distributions with BJH (Barrett–Joyner–Halenda) pore diameters of 31 and 55 Å, respectively (see Supporting Information, Figures S2B and S3B). From measured lattice spacings and pore diameters, the wall thicknesses of MCM-41 and SBA-15 were 13 and 51 Å, respectively.

Composition of the materials was checked using ^{29}Si CP-MAS solid-state NMR spectroscopy, which showed Q3 and Q4 silicon sites centered at about −101 and −115 ppm, respectively. The ^{13}C CP-MAS solid-state NMR spectroscopy did not show peaks corresponding to residual unhydrolyzed ethoxy groups and surfactant templates. These results are consistent with reported physical properties for such materials.[17–19]

Oxygen concentration was measured from the decay of phosphorescence from a palladium phosphor.[20] Cells (0.5×10^6/mL) were suspended in media plus 2 μM Pd phosphor and 0.5% fat-free bovine serum albumin with and without 500 μg/mL MCM-41 or SBA-15, and placed in closed 1 mL vessels for O_2 measurement. Results are in Figure 2A. The rate of cellular mitochondrial O_2 consumption (k, in μM O_2/min) is the negative of the slope in a plot of $[O_2]$ vs t. For untreated cells, $k = 0.64$ ($r^2 = 0.988$); for cells treated with MCM-41, $k = 0.66$ ($r^2 = 0.990$); for cells treated with SBA-15, $k = 0.32$ ($r^2 = 0.961$, 49% inhibition). The k-values for cell-free media containing MCM-41 or SBA-15 were 0.04 or −0.01, respectively (similar to instrument drift). Thus, the interaction between nanoparticles and O_2 or Pd phosphor is negligible.

Dependence of the inhibition on SBA-15 dosing is shown in Figure 2B. The k-value (μM O_2/min) for untreated cells was 0.78 ($r^2 = 0.987$), for cells treated with 50 μg/mL 0.58 ($r^2 = 0.984$, 26% inhibition), for cells treated with 100 μg/mL 0.52 ($r^2 = 0.990$, 33% inhibition), for cells treated with 200 μg/mL 0.50 ($r^2 = 0.959$, 36% inhibition), and for cells treated with 300 μg/mL 0.46 ($r^2 = 0.945$, 41% inhibition). In another experiment, the inhibition with 25 μg/mL SBA-15 was 10%. We have fitted percent inhibition (I) to the function $\alpha d/(\beta + d)$, where d is the dose in μg/mL. The best-fit curve ($r^2 = 0.986$, see Supporting Information, Figure S4) gives $\alpha = 57.8\%$ (maximum inhibition) and $\beta = 102.3$ μg/mL (dose giving to ½ maximum inhibition). Assuming that $I = 0$ for zero dose and I approaches 100% for a very large dose, we also fitted the results to $I = 100[1 - \exp(-ad^b)]$; least-squares fitting ($r^2 = 0.955$) gives $a = 0.0429$ and $b = 0.4454$.

To measure dependence of I on incubation time with SBA-15, every hour samples were withdrawn simultaneously from four conditions, either untreated or treated with 50, 100, or 200 μg/mL SBA-15. Oxygen measurements were then made every minute alternately on all four samples for about an hour, giving the results of Figure 2C (results for 100 μM not shown for clarity). The incubation with the particles thus continued during the measurements. The k-values for all conditions, with statistical errors from linear fitting, are given in Table 1 and Figure 5 in Supporting Information. For 50 μg/mL SBA-15, the inhibitions I at hours 1–6 were 27%, 36%, 9%, 53%, 0%, and 0%. For 100 μg/mL SBA-15, I-values at hours 1–6 were 25%, 25%, 26%, 68%, 0%, and 0%. For 200 μg/mL SBA-15, I-values at hours 1–6 were 64%, 38%, 34%, 51%, 0%, and 46%. Because the statistical errors in k-values are ~10% (see Supporting Information), there is a large uncertainty in each calculated I-value. Therefore, we do not consider a big fluctuation in I from hour h to hour $h + 1$ as meaningful, unless it persists at hour $h + 2$. In another experiment (Table 2 in Supporting Information), inhibition was again significantly greater for higher concentrations and disappeared after a few hours at lower concentrations. Thus, the inhibition is time-dependent as well as dose-dependent, showing recovery with lower concentrations. Cyanide gave almost complete permanent inhibition; after 2 h, the inhibition averaged >94% (Table 2 in Supporting Information), showing O_2 consumption was due to oxidations in the mitochondrial respiratory chain.

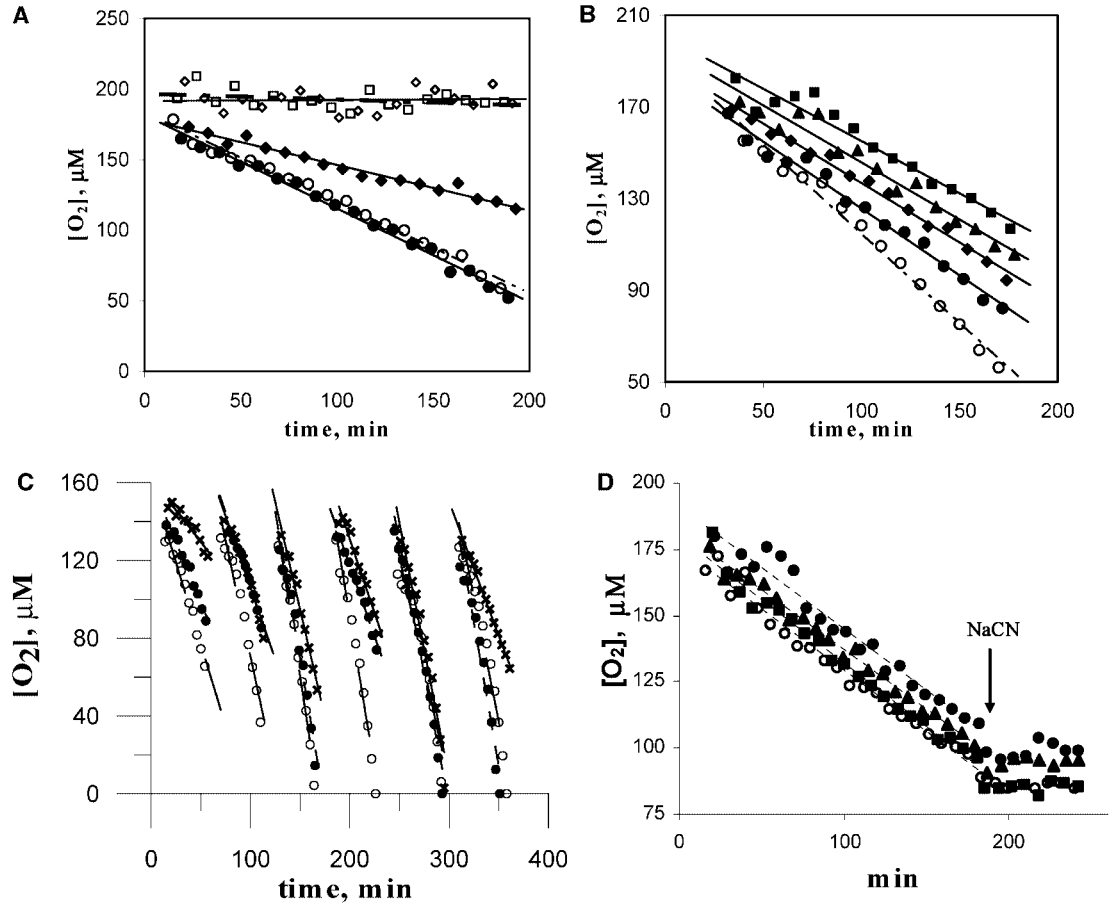

Figure 2. Effects of silica nanoparticles on Jurkat cell respiration. Respiration rate (k) is the negative of the slope when plotting $[O_2]$ vs t, measured in a closed vessel. (A) Respiration was measured in cells (0.5×10^6 per mL) without (open circles and dashed line) or with 500 μg/mL MCM-41 (filled circles and line) or SBA-15 (filled diamonds and line). Open diamonds and open squares are for medium + SBA-15 and medium + MCM-41, respectively. Lines are linear fits. (B) Respiration was measured in cells (0.5×10^6 per mL) without (open circles) or with 50 (closed circles), 100 (diamonds), 200 (triangles), or 300 (squares) μg/mL SBA-15. Lines are linear fits. (C) Cells were suspended at 10^6 cells per mL without or with 50, 100, or 200 μg/mL SBA-15. Samples of all four were taken simultaneously every hour for measurement of $[O_2]$, alternately on each of the four samples, with results shown. Open circles and dashed line = untreated, closed circles and line = 50, crosses and line = 200; 100 μg/mL not shown. (D) $[O_2]$ vs t for cells (0.5×10^6 per mL) exposed to 0 (open circles), 50 (closed circles), 100 (diamonds), or 200 (triangles) μg/mL MCM-41. Lines are linear fits. Injections of 10 mM NaCN at ~185 min halted respiration.

Figure 2D shows the effects of 50, 100, and 200 μg/mL MCM-41 on Jurkat cell respiration. The k-value (μM O_2/min) for untreated cells was 0.46 ($r^2 = 0.977$), for cells treated with 50 μg/mL 0.45 ($r^2 = 0.990$), for cells treated with 100 μg/mL 0.48 ($r^2 = 0.981$), and for cells treated with 200 μg/mL 0.46 ($r^2 = 0.959$). Thus, MCM-41 does not inhibit respiration at any of the concentrations used. For all conditions, respiration was almost completely inhibited by 10 mM NaCN, injected at hour 3.

In other experiments, Jurkat cells were incubated at 37 °C in phosphate-buffered saline (PBS) for 12 h to deplete endogenous metabolic fuels. Then O_2 measurements were performed on (1) cells without glucose, (2) cells with 100 μM glucose, (3) cells with 100 μM glucose plus 50 μg/mL nanoparticles, and (4) cells with 100 μM glucose plus 200 μg/mL nanoparticles. Cell viability at the time of O_2 measurement was >90%. For all conditions, NaCN was added to terminate respiration when $[O_2]$ approached 40 μM. Figure 3 shows the effect of SBA-15, with lines being the best fits to the three-line function:

$$[O_2] = a + bt, \qquad t < t_1$$
$$[O_2] = c + dt, \qquad t_1 \le t \le t_2$$
$$[O_2] = e, \qquad t > t_2$$

Here, t_1 is the onset of accelerated respiration; t_2 is just after the time of NaCN addition. Continuity requires $a + bt_1 = c + dt_1$, and $c + dt_2 = e$, reducing the number of parameters from seven to five. The rate of respiration, k, is equal to $-b$ for $t < t_1$ and $-d$ for $t_1 \le t \le t_2$.

In the absence of glucose, the k-values (μM O_2/min) were 0.18 for $0 < t < 56$ min, 0.38 for $56 < t < 300$ min ($r^2 > 0.995$, 2.1-fold increment), and 0.02 for $t > 300$ min (95% inhibition by NaCN). Presumably, the increased respiration after $t_1 = 56$ min was due to residual intracellular nutrients and fatty acids in the albumin preparation. In the presence of glucose without SBA-15, the k-values were 0.39 for $0 < t < 68$ min, 0.94 for $68 < t < 147$ min ($r^2 > 0.998$, 2.4-fold

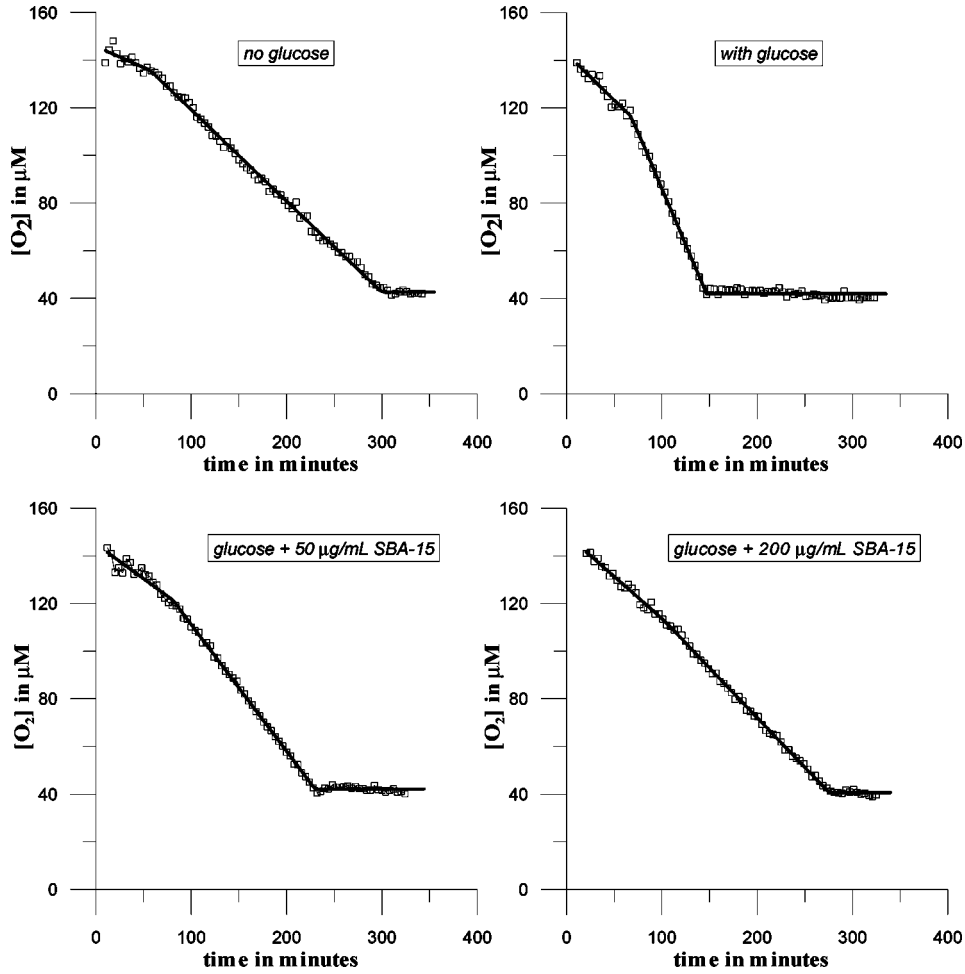

Figure 3. Effects of SBA-15 on glucose-supported respiration in Jurkat cells depleted of metabolic fuels. Cells (10^6 per mL) were washed twice in PBS and incubated at 37 °C in PBS for 12 h to deplete endogenous metabolic fuels. The cells were then suspended in PBS, 2 μM Pd phosphor, and 0.5% albumin with and without 100 μM glucose and 50 or 200 μg/mL SBA-15. When used, glucose and nanoparticles were both added at $t = 0$. Other additions were 10 mM NaCN, added when [O_2] reached 40 μM, which completely stopped O_2 consumption, showing O_2 was consumed in the mitochondrial respiratory chain.

increment), and 0.02 for $t > 147$ min (98% inhibition by NaCN). In the presence of glucose and 50 μg/mL SBA-15, the k-values were 0.29 for $0 < t < 80$ min, 0.53 for $80 < t < 230$ min ($r^2 > 0.998$, 1.8-fold increment), and 0.02 for $t > 230$ min (96% inhibition by NaCN). In the presence of glucose and 200 μg/mL SBA-15, the k values were 0.35 for $0 < t < 102$ min, 0.42 ($r^2 > 0.998$, 1.2-fold increment) for $102 < t < 277$ min, and 0.04 for $t > 277$ min (90% inhibition by NaCN). Thus, t_1 (onset of accelerated respiration) with glucose alone was 68 min, with glucose plus 50 μg/mL SBA-15 80 min (12-min delay), and with glucose plus 200 μg/mL SBA-15 102 min (34-min delay). Moreover, glucose-supported respiration was inhibited 44% by 50 μg/mL SBA-15 and 56% by 200 μg/mL SBA-15.

A similar set of experiments was carried out with MCM-41 (see Supporting Information, Figure S6). In the absence of glucose, no appreciable increase in respiration rate was observed; the best-fit value of t_1 was 26 min. The k-value (μM O_2/min) for $26 < t < 310$ min was 0.18 ($r^2 > 0.981$) and for $t > 310$ min 0.03 (83% inhibition by NaCN). In the presence of glucose without MCM-41, t_1 was 22 min and k for $22 < t < 296$ min was 0.40 ($r^2 > 0.995$) and for $t > 296$ min 0.02 (95% inhibition by NaCN). In the presence of glucose plus 50 μg/mL MCM-41, t_1 was 32 min and k for $32 < t < 301$ min was 0.47 ($r^2 > 0.997$) and for $t > 301$ min 0.01 (98% inhibition by NaCN). With 200 μg/mL SBA-15, t_1 was 49 min and k was 0.40 ($r^2 > 0.996$) for $49 < t < 307$ min and 0.05 for $t > 310$ min (88% inhibition by NaCN). In all conditions with glucose, the k-values were 0.42 ± 0.04 (2.3-fold that without glucose) and reduced to almost zero by NaCN. Thus, MCM-41 had no noticeable effect on respiration rate, but the onset of accelerated respiration was delayed by 10 min by 50 μg/mL MCM-41, and by 27 min by 200 μg/mL MCM-41. Although both SBA-15 and MCM-41 delayed glucose-supported respiration in cells previously depleted of nutrients, only SBA-15 inhibited respiration.

Experiments similar to those on Jurkat cells were performed on HL-60 cells. The effects of SBA-15 on respiration are shown in Figure 4. Figure 4A presents [O_2] vs t for untreated cells and cells treated with 50, 100, or 200 μg/mL. The k-value (μM O_2/min) for untreated cells was 0.44 ($r^2 > 0.995$); for cells treated with 50 μg/mL, 0.29 ($r^2 = 0.975$, 34% inhibition); for cells treated with 100 μg/mL, 0.28 ($r^2 = 0.982$, 36% inhibition); and for cells treated with

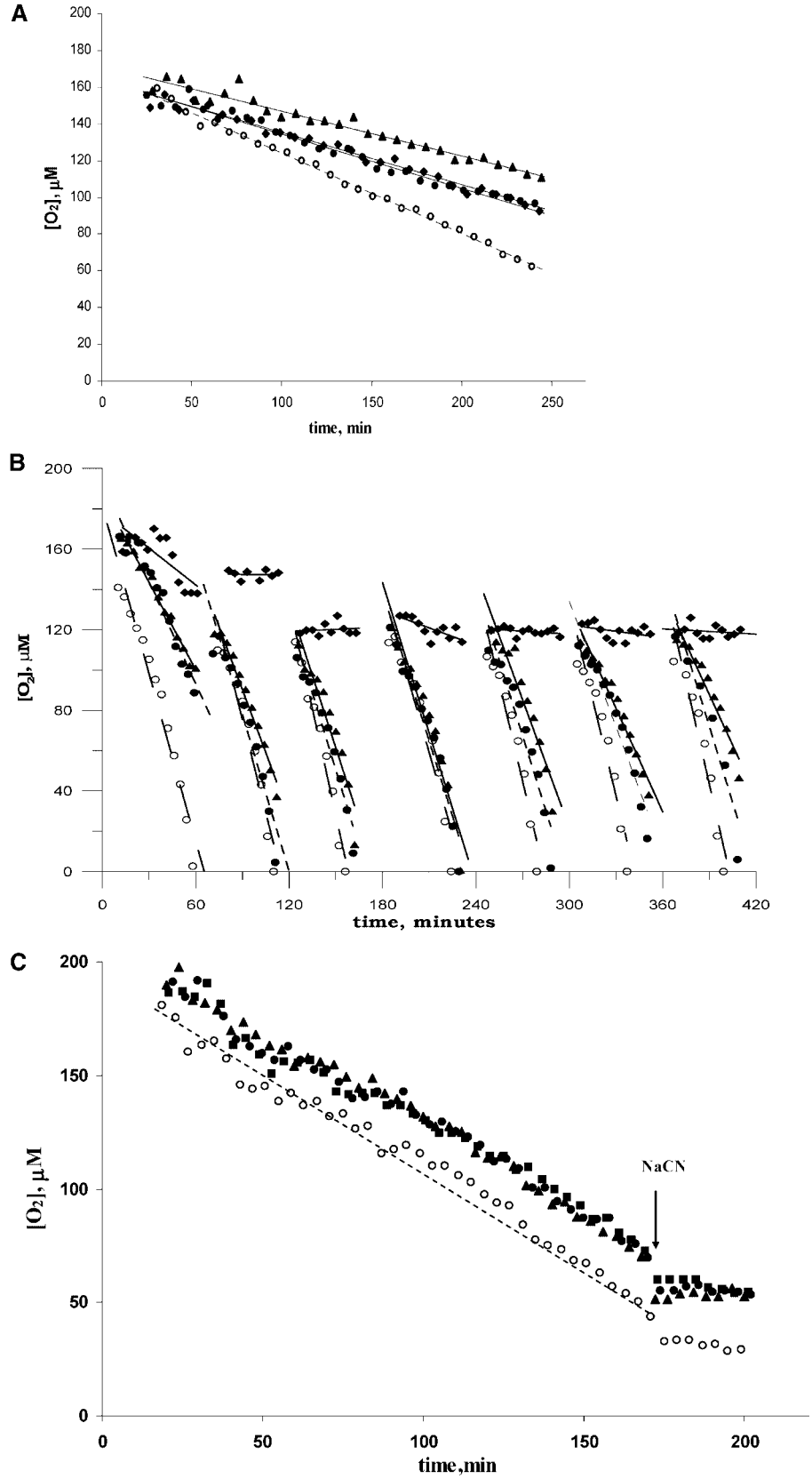

Figure 4. Effects of silica nanoparticles on HL-60 cell respiration. (A) Respiration was measured in cells (0.5×10^6 per mL) without (open circles) or with 50 (closed circles), 100 (diamonds), or 200 (triangles) μg/mL SBA-15. Minute zero corresponds to the addition of particles. Best-fit lines are shown; k is the negative of the slope. (B) Cells were suspended at 10^6 cells per mL without (open circles) or with 50 μg/mL SBA-15 (closed circles), 200 μg/mL SBA-15 (triangles), or 10 mM NaCN (diamonds). Samples were taken simultaneously every hour for all conditions and placed in closed containers for measurement of respiration. Values of k, derived from the linear fits (long-dashed for without SBA-15, short-dashed for 50 μg/mL, solid for 200 μg/mL SBA-15 and for NaCN) are given in Table 3 of Supporting Information. (C) Respiration was measured in cells (0.5×10^6 per mL) without (open circles) or with 50 (solid triangles), 100 (squares), or 200 (diamonds) μg/mL MCM-41. Best linear fits are shown. The addition of 10 mM NaCN was at 3 h.

200 μg/mL, 0.24 ($r^2 = 0.954$, 46% inhibition). The inhibitions are similar to those measured for Jurkat cells (Figure 2B).

Figure 4B shows how respiration rate varies with incubation time with SBA-15 at two concentrations. After 1 h, percent inhibition was 36.0 ± 14.6 (mean ± standard deviation) at 200 μg/mL and 25.0 ± 10.7 at 50 μg/mL; these results were similar to those for Jurkat cells, Figure 2C. There was no sign of recovery out to 7 h. Cyanide inhibited respiration almost completely after 1 h; the average percent inhibition was 95.9 ± 3.8. Detailed results are in Table 3 of Supporting Information.

The effect of MCM-41 on HL-60 respiration (10^6 cells per mL) is shown in Figure 4C. The k-value (μM O_2/min) for untreated cells was 0.81 ($r^2 > 0.984$), for cells treated with 50 μg/mL 0.80 ($r^2 = 0.990$), for cells treated with 100 μg/mL 0.73 ($r^2 = 0.984$), and for cells treated with 200 μg/mL 0.77 ($r^2 = 0.983$). The k-values for all concentrations were essentially the same (0.77 ± 0.03) and not significantly different from the k-values of untreated cells. Apparently, MCM-41 had minimal effect on HL-60 cell respiration. For all conditions, O_2 consumption was inhibited by 10 mM NaCN.

We next investigated the effect of nanoparticles on cellular ATP level. ATP was measured using the luciferin/luciferase bioluminescence system.[8,9] Jurkat and HL-60 cells (0.5×10^6/mL) were incubated at 37 °C with no addition or with 50 μg/mL SBA-15, 50 μg/mL MCM-41, or 10 mM NaCN. Samples were taken from each condition at 0.25, 0.5, 1, 2, and 4 h for ATP determination. Results for Jurkat cells are shown in Figure 5A. Measured ATP concentrations are plotted vs incubation time; each is the average of three to five determinations, with the error bars giving standard deviations. For untreated cells, the best-fit line, shown dashed, had a slope (in nanomoles ATP per 0.5×10^6 cells h^{-1}) of 0.100 ± 0.080 (essentially zero). The slopes were also zero for cells treated with SBA-15, MCM-41, and NaCN; their values being 0.078 ± 0.134, −0.079 ± 0.090, and 0.033 ± 0.051, respectively. Thus, time-average ATP concentrations were calculated, using six points for untreated cells and five points (for $t > 0$) for the other conditions. They were (mean ± standard deviation, in nanomoles of ATP per 0.5×10^6 cells) 2.36 ± 0.28 for untreated, 2.24 ± 0.32 for SBA-15, 2.53 ± 0.42 for MCM-41, and 1.45 ± 0.44 for NaCN. Thus, neither SBA-15 nor MCM-41 at 50 μg/mL significantly affected cellular ATP over 4 h (other experiments, not shown, extended this to 6 h). Cyanide, on the other hand, decreased cellular ATP by 39% within 1 h. Similar results were noted with HL-60 cells (Figure 5B), although statistical errors were somewhat larger than those for Jurkat cells. Since the slope was close to zero (0.179 ± 0.063 nanomoles of ATP h^{-1}), time averages were calculated, using six points for untreated cells and five points for the other conditions. Average cellular ATP levels (mean ± standard deviation, in nanomoles of ATP per 0.5×10^6 cells) were 2.14 ± 0.33 for untreated cells, 2.31 ± 0.77 for SBA-15, 2.23 ± 0.66 for MCM-41, and 1.33 ± 0.38 for NaCN.

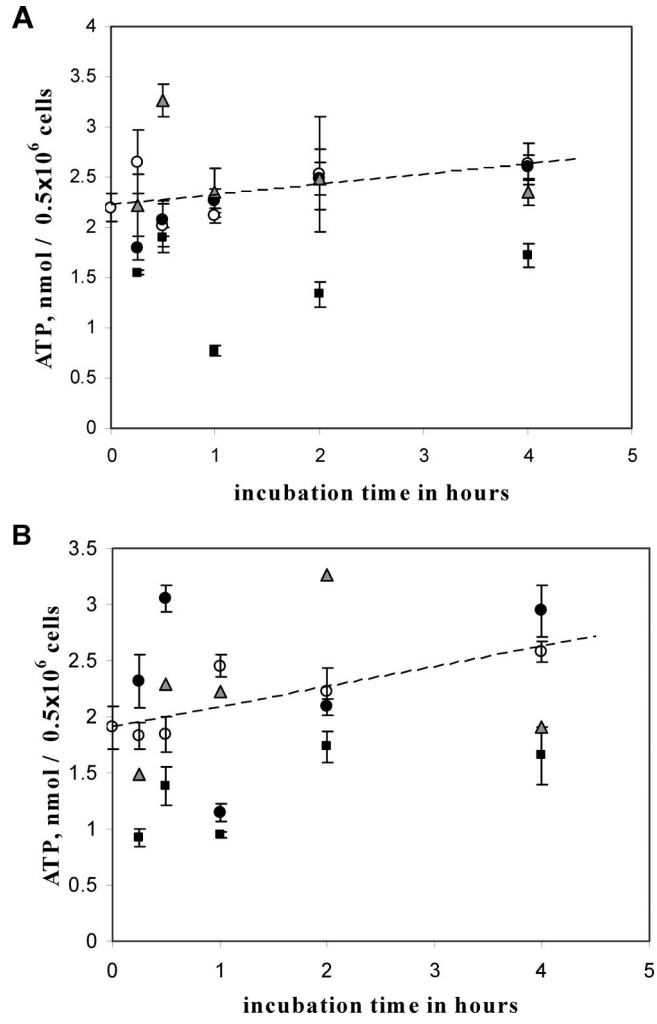

Figure 5. Effects of silica nanoparticles on cellular ATP. (A) Jurkat cells (0.5×10^6 per mL) were incubated at 37 °C for indicated periods of time without additions (open circles) or with 50 μg/mL SBA-15 (closed circles), 50 μg/mL MCM-41 (triangles), or 10 mM NaCN (squares). Measured ATP concentrations are plotted vs incubation time; each is the average of three to five determinations, with the error bars giving standard deviations. Since the slope of the best-fit line for untreated cells (dashed) has slope ~0, time-average ATP concentrations were calculated. (B) HL-60 cells (0.5×10^6 per mL) were incubated at 37 °C for indicated periods of time without additions (open circles) or with 50 μg/mL SBA-15 (closed circles), 50 μg/mL MCM-41(triangles), or 10 mM NaCN squares). The best-fit line (dashed) for untreated cells has a very small slope, so average ATP levels were calculated as for Jurkat cells.

At 200 μg/mL, SBA-15, but not MCM-41, significantly diminished cellular ATP (Figure 6A). For untreated HL-60 cells the average ATP level over time (mean ± standard deviation in nanomoles of ATP per 0.5×10^6 cells) was 0.725 ± 0.054. For MCM-41 treated cells the ATP level deviated by more than the standard deviation from the level for untreated cells only once (at hour 4), implying a random error, rather than a real decrease. Including all points, the average ATP level for MCM-41 treated cells was 0.661 ± 0.116, equal to that for untreated cells within standard error. For SBA-15 treated cells, the ATP level was 23% lower at hour 1 ($p < 0.04$), 41% lower at hour 2 ($p < 0.02$); decreases at hours 3–6 were 24%, 14%, 28%, and −2% (i.e., zero).

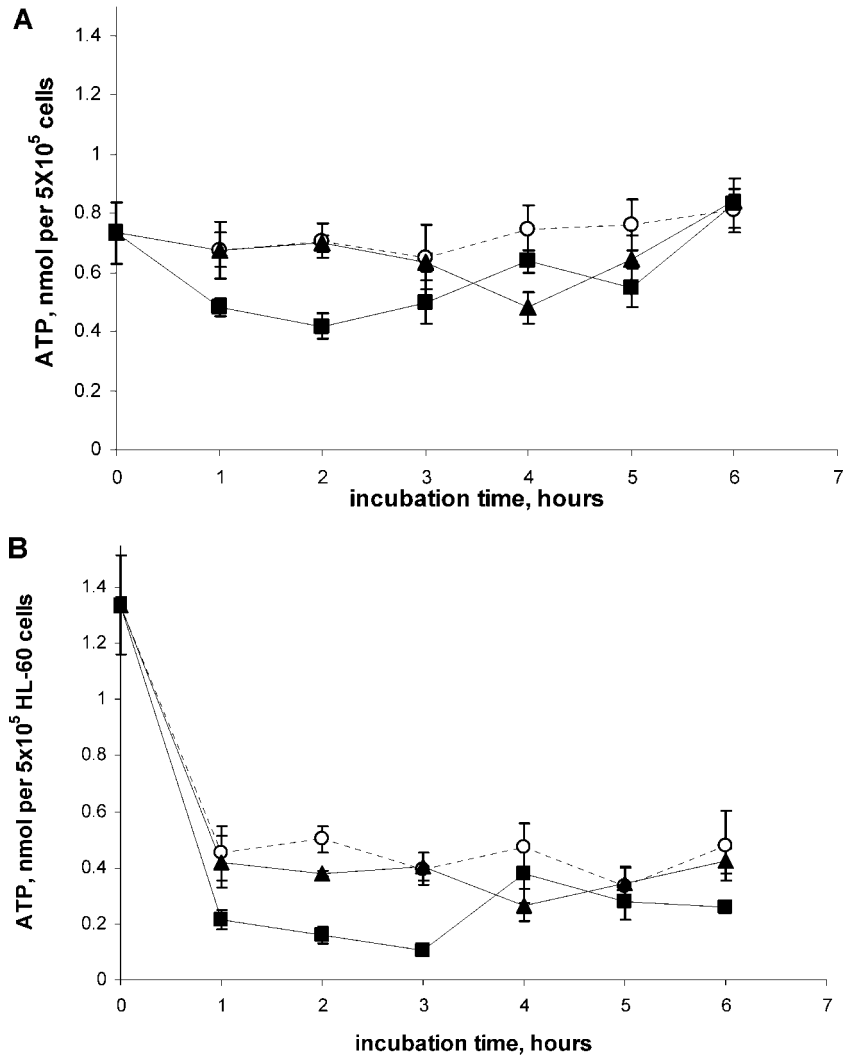

Figure 6. (A) HL-60 cells (0.5×10^6 per mL) were incubated at 37 °C for indicated periods of time without or with 200 μg/mL SBA-15 or 200 μg/mL MCM-41. ATP levels were measured three to five times for each condition at $t = 1$–6 h. Open circles, no addition; filled squares, 200 μg/mL SBA-15; filled triangles, 200 μg/mL MCM-41. (B) The experiment in panel A was repeated in the presence of 10 mM NaCN. Open circles, NaCN alone; closed squares, NaCN plus 200 μg/mL SBA-15; closed triangles, NaCN plus 200 μg/mL MCM-41. Standard deviations are indicated with error bars.

The average decrease between 1 and 5 h was 27%, with full recovery at hour 6. These results parallel the temporary inhibition of HL-60 respiration by SBA-15 (Figure 4B).

The above experiment was repeated in the presence of 10 mM NaCN (Figure 6B). Cyanide decreased cellular ATP in all conditions. The time-average cellular ATP level for $t > 0$ (mean $\pm$ standard deviation in nanomoles of ATP per 0.5×10^6 cells) with NaCN alone was 0.434 ± 0.093, with NaCN plus MCM-41 0.377 ± 0.076 (13% decrease, probably not statistically significant), and with NaCN plus SBA-15 0.232 ± 0.102 (47% decrease, which is significant). This shows that ATP hydrolysis (consumption) occurred in all conditions, and even faster with SBA-15 present.

The effects of nanoparticles on cellular GSH were also studied. Jurkat and HL-60 cells (10^6 per mL) were left untreated or treated at 37 °C for up to 4 h with 50 μg/mL SBA-15 or MCM-41. Samples were taken every hour for measurement of cellular GSH. The results, shown in Figure S9 (Supporting Information), suggest that the effect of these nanoparticles on cellular GSH was minimal. In other experiments, cells were incubated at 37 °C for 6 h without or with 50 μg/mL SBA-15, 50 μg/mL MCM-41, or 5 mM NEM (which rapidly reacts with GSH, preventing mBBr labeling). Results (mean $\pm$ standard deviation for three measurements in each case) are shown in Figure S9C (Jurkat cells) and Figure S9D (HL-60 cells). Although NEM completely blocked mBBr labeling, no significant changes in cellular GSH ($p > 0.09$) were noted with 50 μg/mL of either SBA-15 or MCM-41. Even at 200 μg/mL, neither nanoparticle had a significant effect on cellular GSH after a 6 h incubation (data not shown).

Finally, we evaluated the effects of nanoparticles on respiration of isolated mitochondria and submitochondrial particles (SMP). Mitochondria or SMP were suspended in 10 mM Tris-Cl (pH 8.2), 250 mM sucrose, 2 μM Pd phosphor, and 0.5% albumin with and without SBA-15 or MCM-41. Concentrations of 50, 100, and 200 μg/mL were used for both nanoparticles. Succinate (10 mM) was added

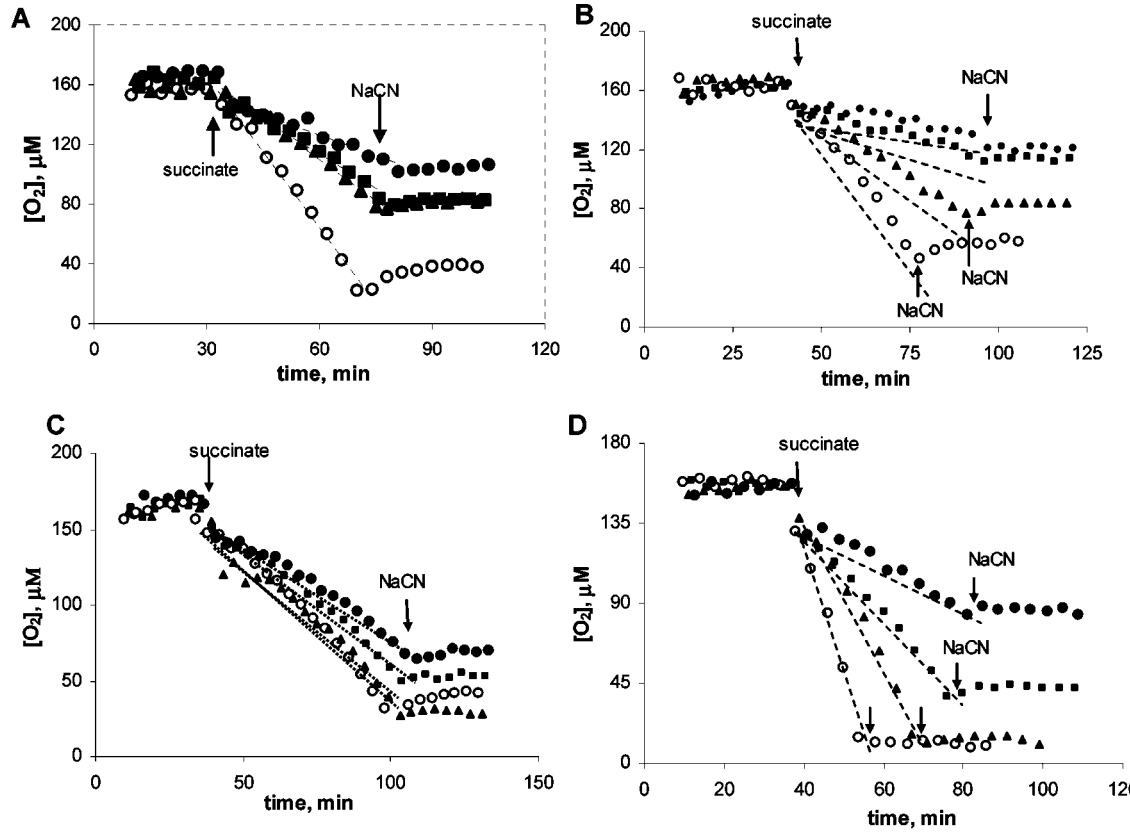

Figure 7. Effects of nanoparticles on respiration of isolated mitochondria and submitochondrial particles (SMP). Mitochondria or SMP (15–20 μg/mL) were suspended in 10 mM Tris-Cl (pH 8.2), 250 mM sucrose, 2 μM Pd phosphor, and 0.5% albumin with and without SBA-15 (A, mitochondria; B, SMP) or MCM-41 (C, mitochondria; D, SMP). Concentrations of 0 (open circles), 50 (triangles), 100 (squares), and 200 (closed circles) μg/mL were used for both nanoparticles. Zero minutes corresponds to the addition of nanoparticles. Succinate (10 mM) was added to initiate respiration and NaCN (10 mM) to terminate respiration.

at $t \sim 30$ min to initiate respiration and NaCN (10 mM) was added later on to terminate respiration. The results of one set of experiments are given in Figure 7; when these experiments were repeated, results (k-values) were quite comparable to those in Figure 7. The same was true for the cell respiration experiments.

For SBA-15 and mitochondria (Figure 7A), [O_2] was monitored continuously to 100 min. Oxygen concentrations for $30 < t < 75$ min were fitted to straight lines. The k-value (μM O_2/min) for mitochondria without SBA-15 was 3.38 ($r^2 = 0.986$), for mitochondria with 50 μg/mL 1.83 ($r^2 = 0.987$), for mitochondria with 100 μg/mL 1.51 ($r^2 = 0.962$), and for mitochondria with 200 μg/mL 0.92 ($r^2 = 0.942$). These values correspond, respectively, to inhibitions of 46%, 55%, and 73%. Figure 7B shows [O_2] for treated and untreated SMP. The k-value for untreated SMP was 2.96 ($r^2 = 0.990$), for SMP treated with 50 μg/mL 1.56 ($r^2 = 0.997$), for SMP treated with 100 μg/mL 0.64 ($r^2 = 0.948$), and for SMP treated with 200 μg/mL 0.41 ($r^2 = 0.882$). These correspond to inhibitions of 47%, 78%, and 86%, respectively.

For MCM-41 and mitochondria (Figure 7C), [O_2] was monitored continuously out to 130 min, with 10 mM succinate added at $t = 40$ min and NaCN at $t = 100$ min. Results for $40 < t < 100$ min were fitted to lines to obtain k-values. The k-value (μM O_2/min) for untreated mitochondria was 2.43 ($r^2 = 0.993$), for mitochondria treated with 50 μg/mL 1.17 ($r^2 = 0.965$), for mitochondria treated with 100 μg/mL 1.20 ($r^2 = 0.978$), and for mitochondria treated with 200 μg/mL 1.08 ($r^2 = 0.987$). These values correspond to inhibitions of 52%, 51%, and 56%, respectively. Figure 7D shows the results for SMP, untreated or treated with MCM-41. The k-value for untreated SMP was 7.20 ($r^2 = 0.985$), for SMP treated with 50 μg/mL 4.22 ($r^2 = 0.984$), for SMP treated with 100 μg/mL 2.46 ($r^2 = 0.989$), and for SMP treated with 200 μg/mL 1.23 ($r^2 = 0.971$). These correspond to inhibitions of 41%, 66%, and 83%, respectively. In all conditions, O_2 consumption was completely inhibited with NaCN.

Cellular respiration includes the delivery of O_2 to mitochondria, the breakdown of reduced fuels (e.g., succinate) with passage of electrons to O_2 (forming H_2O), and the resulting synthesis of ATP. Toxins frequently target mitochondria and impair oxidative phosphorylation. We have measured cellular respiration and ATP content in the presence of two types of mesoporous silica nanoparticles, SBA-15 and MCM-41 (Figure 1). Cyanide markedly inhibited respiration and ATP content, establishing that both processes occurred in association with oxidations in the respiratory chain. Thus, reactive oxygen species did not contribute significantly to the observed O_2 consumption. That cellular GSH remained unchanged (Figure S7 in Supporting

Information) in the presence of nanoparticles further confirmed the negligible role of ROS.

Our results show SBA-15 interferes with cellular respiration, whereas MCM-41 has no effect (Figure 2). This must be connected with the different physical properties of mesoporous silica nanoparticles (e.g., shape, size, and pores, Figures S1−S3). Inhibition is proportional to dosing for concentrations $\leq 100\ \mu$g/mL but levels off thereafter (Figure S4 in Supporting Information). This may suggest that not all mitochondria are equally susceptible to SBA-15 (e.g., mitochondria near the cell membrane may be more vulnerable). The mitochondrial injury also depends nonmonotonically on incubation time with SBA-15 (Figure 2C). For 50 or 100 μg/mL SBA-15, the impairment of respiration increased with exposure time up to 3 h and then decreased, indicating time-dependent inhibition, with recovery. The time dependence of cellular ATP (Figure 6A) paralleled that of inhibition of cellular respiration. For 200 μg/mL, the inhibition did not decrease at long times, indicating recovery was impossible for cells exposed to this high concentration.

If the particles are considered to be spheres of diameter 500 nm and density 2.5 g/cm^3, each particle has a mass of 1.64×10^{-13} g, and 200 μg/mL corresponds to 1.22×10^9 particles/mL. With 10^6 cells per mL, this means 1200 particles per cell. The mean Jurkat cell volume, determined on the Coulter model Z2 (Beckman Coulter, Inc.) was 1.7×10^{-13} L, which is 2600 times the volume of a nanoparticle. The surface area of a Jurkat cell is calculated, assuming spherical cells with radius 3.4×10^{-6} m, as 1.5×10^{-10} m^2, which is 760 times the cross-sectional area of a nanoparticles. However, it is not known whether the particles are internalized or attached to the cell surface. We did, however, perform a number of experiments to elucidate the mechanism of respiration inhibition.

First, we measured respiration of cells depleted of metabolic fuels (Figure 3). Introduction of glucose led to an increase in respiration rate, but not immediately. The delay (t_1) reflects the time required for cellular glucose uptake, generation of reduced metabolic fuels via glycolysis, transport of the fuels into the mitochondria, etc. At a later time (t_2) NaCN was injected to shut down respiration. We fitted measured [O_2] as a function of t to a three-line function, with the third line horizontal. This involved choosing values of five parameters, including k (rate of respiration), t_1, and t_2, to produce the best fit.. With 50 μg/mL SBA-15, t_1 increased by 12 min and k decreased by 44%; the corresponding numbers for 200 μg/mL SBA-15 were 34 min and 56% (Figure 3A). These results confirm concentration-dependent interference by SBA-15 in glucose-supported respiration. With MCM-41, there was little effect on the k-values (Figure S6 in Supporting Information). However, there was an increase in the delay time t_1 with increasing MCM-41 concentration, similar to that of SBA-15 (Figure 3). Thus MCM-41 affects glucose processing but not respiration.

Second, we measured cellular ATP levels in the presence of 50 or 200 μg/mL nanoparticles. There was little change in ATP concentration with time with 50 μg/mL of either nanoparticle, whereas cyanide decreased cellular ATP by 39% within 1 h (Figure 5). However, 200 μg/mL SBA-15 (but not MCM-41) significantly diminished cellular ATP (Figure 6A). Compared to untreated cells, the ATP level in SBA-15-treated cells was 23% lower at hour 1, 41% lower at hour 2, and fully recovered at hour 6. This parallels the inhibition profile of SBA-15 on respiration (Figure 2C). The results with cyanide present of Figure 6B confirm that ATP hydrolysis (consumption) is not significantly altered in the nanoparticle-treated cells.

Third, cellular GSH was measured without and with 50 μg/mL SBA-15 or MCM-41 (Figure S7A-B in Supporting Information). Measurements were made on samples taken every hour and the results fitted to exponentials. The values of the exponential parameters were about the same for the three conditions in both cell types, suggesting minimal effect of nanoparticles on cellular GSH. Even at a nanoparticle concentration of 200 μg/mL, there was no significant effect on cellular GSH at 6 h (Figure S7 C-D in Supporting Information). Thus, it is unlikely that significant ROS was generated in the nanoparticle-treated cells.

Finally, we measured the respiration of mitochondria and SMP (prepared by sonication of mitochondria) in the presence of the nanoparticles (Figure 7). For the SMP, the substrate (succinate) is in direct contact with complex II of the respiratory chain, whereas substrate delivery is needed for the mitochondria. (To test this definitively, intact rat liver mitochondria exhibiting a high level of respiratory control are necessary.) Both SBA-15 and MCM-41 were equally toxic to the mitochondria and SMP.

Thus, it appears that the physical properties of nanoparticles determine their effects on cellular bioenergetics. Cyanide-sensitive oxidative phosphorylation is inhibited in cells exposed to SBA-15, which has lower specific surface, larger size, and larger pores than MCM-41. Although its smaller pores may limit entry of essential biomolecules, MCM-41 has only a small effect on cellular respiration. Our results suggest that the minimal effect of MCM-41 is likely due to limited access to cellular mitochondria. The cellular uptake of MCM-41 may be hindered by its high surface area per unit mass.

Acknowledgment. This work is supported by a fund from Paige's Butterfly Run. T.A. acknowledges financial support from the National Science Foundation (NSF), CHE-0645348.

Supporting Information Available: Descriptions of the syntheses of MCM-41 and SBA-15, plus characterization by TEM, XRD, NGAI, and solid-state NMR spectroscopy, detailed procedures of cellular and mitochondrial experiments, including oxygen consumption, ATP formation, and cellular GSH level, and tabulated results of many experiments. This material is available free of charge via the Internet at http://pubs.acs.org.

References

(1) Service, R. *Science* **2005**, *310*, 1609.
(2) Kipen, H. M.; Laskin, D. L. *Am. J. Physiol.: Lung Cell. Mol. Physiol.* **2005**, *289*, L696–L697.

(3) Nel, A.; Xia, T.; Madler, L.; Li, N. *Science* **2006**, *311*, 622–627.
(4) Bottini, M.; Bruckner, S.; Nika, K.; Bottini, N.; Bellucci, S.; Magrini, A.; Bergamaschi, A.; Mustelin, T. *Toxicol. Lett.* **2006**, *160*, 121–126.
(5) Sayes, C. M.; Gobin, A. M.; Ausman, K. D.; Mendez, J.; West, J. L.; Colvin, V. L. *Biomaterials* **2005**, *26*, 7587–7595.
(6) Lin, W.; Huang, Y.-W.; Zhou, X.-D.; Ma, Y. *Toxicol. Appl. Pharmacol.* **2006**, *217*, 252–259.
(7) Hessler, J. A.; Budor, A.; Putchakayala, K.; Mecke, A.; Rieger, D.; Banaszak Holl, M. M.; Orr, B. G.; Bielinska, A.; Beals, J.; Baker, J., Jr. *Langmuir* **2005**, *20*, 9280–9286.
(8) Tao, Z.; Weathers, H.; Penefsky, H. S.; Goodisman, J.; Souid, A.-K. *Chem. Res. Toxicol.* **2006**, *19*, 1051–1058.
(9) Tao, Z.; Syed, A.; Penefsky, H. S.; Goodisman, J.; Souid, A.-K. *Mol. Pharm.* **2006**, *3*, 762–772.
(10) Tao, Z.; Penefsky, H. S.; Goodisman, J.; Souid, A.-K. *Mol. Pharm.* **2007**, *4*, 583–595.
(11) Green, D. R.; Kroemer, G. *Science* **2004**, *305*, 626–629.
(12) Slowing, I.; Trewyn, B. G.; Lin, V. S.-Y. *J. Am. Chem. Soc.* **2006**, *128*, 14792–14793.
(13) Di Pasqua, A. J.; Sharma, K. K.; Shi, Y.-L.; Toms, B. B.; Ouelette, W.; Dabrowiak, J. C.; Asefa, T. *J. Inorg. Biochem.* In press.
(14) Lai, C. Y.; Trewyn, B. G.; Jeftinija, D. M.; Jeftinija, K.; Xu, S.; Jeftinija, S.; Lin, V. S.-Y. *J. Am. Chem. Soc.* **2003**, *125*, 4451–4459.
(15) Tang, Q.-L.; Xu, Y.; Wu, D.; Sun, Y.-H.; Wang, J.; Xu, J.; Deng, F. *J. Controlled Release* **2006**, *114*, 41–46.
(16) Vallet-Regi, M. *Chem. Eur. J.* **2006**, *12*, 5934–5943.
(17) Sharma, K. K.; Asefa, T. *Angew. Chem., Int. Ed.* **2007**, *46*, 2879–2882.
(18) Huh, S.; Wiench, J. W.; Yoo, J. C.; Pruski, M.; Lin, V. S.-Y. *Chem. Mater.* **2003**, *15*, 4247–4256.
(19) Zhao, D. Y.; Huo, Q. S.; Feng, J. L.; Chmelka, B. F.; Stucky, G. D. *J. Am. Chem. Soc.* **1998**, *120*, 6024–6036.
(20) Lo, L.-W.; Koch, C. J.; Wilson, D. F. *Anal. Biochem.* **1996**, *236*, 153–160.
(21) Souid, A.-K.; Newton, G. L.; Dubowy, R. L.; Fahey, R. C.; Bernstein, M. L. *Cancer Chemother. Pharmacol.* **1998**, *42*, 400–406.

NL080250U